Mineralogy and crystal structure of bouazzerite from Bou Azzer, Anti-Atlas, Morocco: Bi-As-Fe nanoclusters containing Fe^{3+} in trigonal prismatic coordination

JOËL BRUGGER,[1,*] NICOLAS MEISSER,[2] SERGEY KRIVOVICHEV,[3] THOMAS ARMBRUSTER,[4] AND GEORGES FAVREAU[5]

[1]Department of Geology and Geophysics, Adelaide University, North Terrace, SA-5001 Adelaide, Australia and South Australian Museum, North Terrace, SA-5000 Adelaide, Australia
[2]Musée Géologique Cantonal and Laboratoire des Rayons-X, Institut de Minéralogie et Géochimie, UNIL-Anthropole, CH-1015 Lausanne-Dorigny, Switzerland
[3]Department of Crystallography, St. Petersburg State University, University Emb. 7/9, 199034 St. Petersburg, Russia
[4]Laboratorium für chemische und mineralogische Kristallographie, Universität Bern, Freiestrasse 3, CH-3012 Bern, Switzerland
[5]421 Avenue Jean Monnet, 13090 Aix-en-Provence, France

ABSTRACT

Bouazzerite, $Bi_6(Mg,Co)_{11}Fe_{14}[AsO_4]_{18}O_{12}(OH)_4(H_2O)_{86}$, is a new mineral occurring in "Filon 7" at the Bou Azzer mine, Anti-Atlas, Morocco. Bouazzerite is associated with quartz, chalcopyrite, native gold, erythrite, talmessite/roselite-beta, Cr-bearing yukonite, alumopharmacosiderite, powellite, and a blue-green earthy copper arsenate related to geminite. The mineral results from the weathering of a Variscan hydrothermal As-Co-Ni-Ag-Au vein. The Bou Azzer mine and the similarly named district have produced many outstanding mineral specimens, including the world's best erythrite and roselite.

Bouazzerite forms monoclinic prismatic {021} crystals up to 0.5 mm in length. It has a pale apple green color, a colorless streak, and is translucent with adamantine luster. d_{calc} is 2.81(2) g/cm^3 (from X-ray structure refinement). The new mineral is biaxial with very weak pleochroism from yellow to pale yellow; the refractive indices measured on the (021) cleavage face range from n_{min} = 1.657 to n_{max} = 1.660; the Gladstone-Dale relationship provides a value of 1.65. The empirical chemical formula is $Bi_{6.14}Fe_{12.6}Mg_{8.45}Co_{0.48}Ni_{0.12}Ca_{0.23}(As_{17.0}Cr_{0.64}Si_{0.32})_{\Sigma=18.0}O_{174.6}H_{184}$. Bouazzerite is monoclinic, $P2_1/n$, $Z = 2$, with $a = 13.6322(13)$ Å, $b = 30.469(3)$ Å, $c = 18.4671(18)$ Å, $\beta = 91.134(2)°$, and $V = 7669.0(13)$ Å^3. The eight strongest lines in the X-ray powder diffraction pattern are [d in Å (I)(hkl)]: 11.79(100)(02$\bar{1}$), 10.98(80)(101/$\bar{1}$01), 10.16(80)($\bar{1}$20), 7.900(80)(02$\bar{2}$), 12.45(70)(1$\bar{1}$0), 15.78(60)(0$\bar{1}$1), 3.414(40)(3$\bar{3}$3/400), 3.153(40)(35$\bar{3}$/2$\bar{2}$5).

The crystal structure of bouazzerite is based upon $[Bi_3Fe_7O_6(OH)_2(AsO_4)_9]^{11-}$ anionic nanoclusters that are built around [$^{trigonal\ prismatic}Fe^{3+}(^{octahedral}Fe_3^{3+}(OH)O_{12})_2]^{29-}$ groups, containing one Fe^{3+} ion in trigonal prismatic coordination and six Fe^{3+} ions in octahedral coordination. The nanoclusters have a diameter of about 1.3 nm and are linked together by chains of $Mg(O,H_2O)_6$ octahedra. The resulting arrangement displays channels down [100] that contain structural water. Bouazzerite is the first mineral based upon Bi- and As-containing ferric nanoclusters. Its discovery provides a unique insight into transport mechanisms of toxic elements in the oxidation zones of sulfide mineral deposits in the form of complex Fe-As nanoparticles.

Keywords: Bouazzerite, new mineral, crystal structure determination, trigonal prismatic coordination, Bou Azzer province, Anti-Atlas, Morocco

INTRODUCTION

The oxidation of polymetallic deposits results in the formation of a great diversity of secondary minerals; deposits like Tsumeb (Namibia) and Broken Hill (Australia) truly are among the mineralogical rainforests of the planet (Pring 1995). The study of the mineralogy of these deposits contributes to our understanding of heavy metal mobility in the near-surface environment, with direct applications to using soil sampling from geochemical prospecting, and as analog for heavy metal mobility around waste

deposits (e.g., Williams 1990). Occasionally, new minerals from this setting present their own intrinsic interest. For example, bernalite Fe(OH)$_3$ from Broken Hill, Australia, represents a surprising addition to the well-known Fe-O-H system, and an interesting perovskite-like structure with A-site vacancy (Birch et al. 1993; Welch et al. 2005).

In this paper, we present a description of the mineralogy and crystal structure of bouazzerite, a new hydrated Mg-Fe-Bi-arsenate from the Bou Azzer mine, Anti Atlas, Morocco. The mineral is remarkable because it contains Bi^{3+}-As^{5+}-Fe^{3+} nanoclusters in which Fe^{3+} exists in trigonal prismatic coordination. Bouazzerite is the first example of trigonal prismatic coordination for a first-

* E-mail: joel.brugger@adelaide.edu.au

row transition metal in an inorganic compound, and the first reported occurrence of complex Bi-As-Fe nanoclusters.

The new mineral name "bouazzerite" recognizes the exceptional significance of the Bou Azzer district and, in particular, of the Bou Azzer mine to mineralogical sciences and mineral collecting. The Bou Azzer district, including from west to east the following ore deposits: Méchoui, Taghouni, Bou Azzer sensu stricto, Aghbar (also spelled Arhbar), Ightem (also spelled Irhtem), Oumlil, Tamdrost and Aït Ahmane, belongs to the world's most famous mineral localities, and has provided the world's best specimens for several species, including erythrite (from "Filon 7;" Jacob and Schubnel 1972), roselite, roselite-beta, skutterudite and gersdorffite. By 2006, around 210 minerals were known from the Bou Azzer district (Favreau and Dietrich 2006), including 7 new minerals: arhbarite, $Cu_2MgAsO_4(OH)_3$, Arhbar mine (Schmetzer et al. 1982; Krause et al. 2003); bouazzerite, Bou Azzer mine (this study; Meisser and Brugger 2006); irhtemite, $Ca_4MgH_2(AsO_4)_4 \cdot 4H_2O$, Ightem and Bou Azzer mines (Pierrot and Schubnel 1972); maghrebite, $MgAl_2(AsO_4)_2(OH)_2 \cdot 8H_2O$, Aghbar mine (Meisser and Brugger 2006); nickelaustinite, $Ca(Ni,Zn)AsO_4(OH)$, Bou Azzer district (Cesbron et al. 1987); smolianinovite, $(Co,Ni,Ca,Mg)_3(Fe,Al)_2(AsO_4)_4 \cdot 11H_2O$, Fleischer 1957); and wendwilsonite, $Ca_2(Mg,Co)(AsO_4)_2 \cdot 2H_2O$, Bou Azzer district (Dunn et al. 1987). The district also provides the second world occurrence for species such as cobaltarthurite, cobaltlotharmeyerite, nickellotharmeyerite, and guanacoite. The name bouazzerite was used in the local mining vernacular to describe a ferroan variety of stichtite, but was discredited early on by Caillères (1942) and again by Paclt (1953). The name was never used in the scientific literature, and the GEOREF database contains only the reference to the discredit by Paclt (1953). The type material is deposited at the Musée Géologique Cantonal, Lausanne, Switzerland (holotype MGL 79798 and cotype MGL 79803).

OCCURRENCE AND ORIGIN

Bouazzerite has been found during recent mining activity at the Bou Azzer As-Co-Ni-Ag-Au deposit in the Anti-Atlas, Morocco. All the samples of bouazzerite were collected in May 2001 from an ore cart freshly extracted from "Filon 7" (French for Vein 7) through "Puits 1" (shaft 1). The ore was particularly rich in native gold, containing up to 100 g/t according to mine geologists. Bouazzerite is directly associated, over a ~1 cm^2 area, with quartz, chalcopyrite, erythrite, Cr-bearing yukonite, alumopharmacosiderite, powellite, and a blue-green earthy copper arsenate related to geminite.

The Bou Azzer deposit (1 350 000 t ore extracted between 1933 and 1995 from "Filon 7" and "Filon 5") formed by hydrothermal remobilization of Ni, Co, Cu, As, and Au from a Proterozoic ophiolite complex during the Variscan Orogeny (Favreau and Dietrich 2001; Leblanc and Billaud 1982). "Filon 7" and "Filon 5" are the main producing veins; "Filon 7" is about 1 km in length, and is located at the contact between a quartz-bearing diorite and a serpentinite (Leblanc 1980). Bouazzerite is a weathering product of As-Ni-Fe-Co-Bi ores hosted in a quartz-carbonate vein matrix. The presence of Cr in bouazzerite also indicates a contribution from the weathering of chromite in the serpentinite rock hosting the vein.

APPEARANCE, PHYSICAL, AND OPTICAL PROPERTIES OF BOUAZZERITE

Bouazzerite occurs extremely rarely as prismatic monoclinic crystals up to 0.5 mm in length. The morphology is dominated by the {021} prism (Figs. 1a and 1b). The crystals are terminated by faces that probably belong to the {110} prism (Fig. 1b). Bouazzerite is pale apple green, with colorless streak and adamantine luster. It is translucent and displays no fluorescence under UV irradiation. The mineral is very brittle with uneven fracture; Mohs' hardness was not determined due to the scarcity of the material. Bouazzerite displays a good cleavage parallel to prism {021} and a fair cleavage parallel to {100} (Fig. 1). The mineral dehydrates quickly under vacuum; this results in a significant contraction and fracturing along the two cleavage directions for crystals observed under the electron scanning microscope or the electron microprobe (Fig. 1). The density could not be measured due to the scarcity of the mineral. The density calculated from the crystal structure refinement is 2.81 g/cm^3, and that calculated from the empirical chemical formula shown in Table 1 is 2.84 g/cm^3.
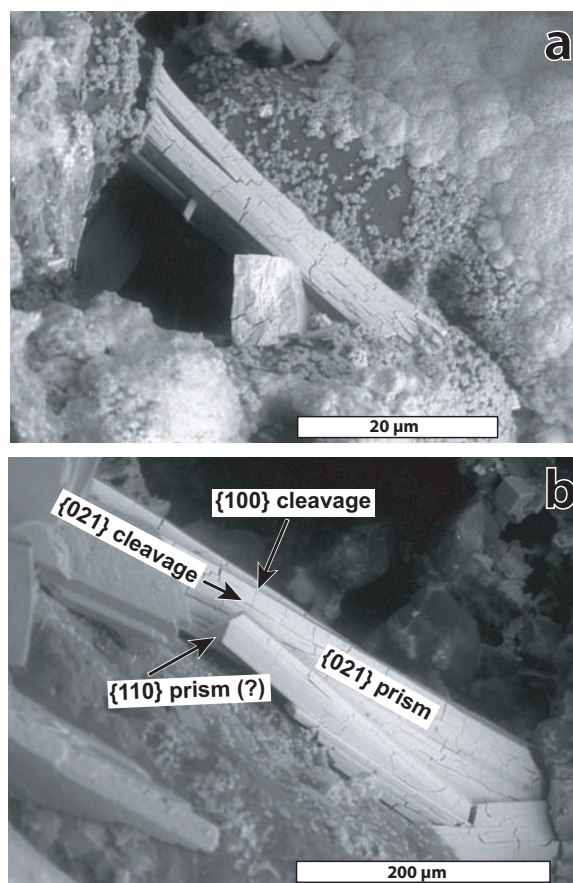
FIGURE 1. Scanning electron micrographs of bouazzerite crystals associated with botryoidal powellite and minute isometric crystals of alumopharmacosiderite. The cracks along the {100} and {021} cleavage directions are caused by dehydration. Measurement conditions: 20 kV, backscattered electron mode, 20 Pa H$_2$O vapor pressure.

TABLE 1. Electron microprobe micro-chemical analysis of bouazzerite

	Average (5 pts)	Range	
As$_2$O$_5$*	35.55	34.29	36.40
CrO$_3$	1.15	0.64	1.84
SiO$_2$	0.35	0.39	0.40
Bi$_2$O$_3$	25.97	25.38	27.69
Fe$_2$O$_3$	18.30	17.58	18.98
MgO	6.18	5.92	6.40
CoO	0.65	0.61	0.68
NiO	0.17	0.07	0.39
CaO	0.23	0.17	0.30
H$_2$O$_{calc}$	30.08	29.71	30.35
Sum	118.6	117.0	119.6
Atoms per formula unit			
As^{5+}	17.04	16.62	17.38
Cr^{6+}	0.64	0.35	1.03
Si^{4+}	0.32	0.26	0.37
Σtet. sites	18.00 (norm)		
Bi^{3+}	6.14	5.95	6.55
Fe^{3+}	12.63	12.13	13.04
Mg	8.45	8.19	8.67
Co	0.48	0.45	0.50
Ni	0.12	0.05	0.29
Ca	0.23	0.17	0.30
Σ	9.28	9.08	9.43
H	184 (norm)		
O	174.6	174.5	174.9

Notes: V$_2$O$_5$ ≤ 0.05 wt%; MnO ≤ 0.12 wt%; SrO ≤ 0.07 wt%; PbO ≤ 0.14 wt%; CuO ≤ 0.14 wt%. No additional element with atomic number ≥9 was detected (<0.1 wt%).
* (wt%).

Optically, bouazzerite is biaxial, with very weak pleochroism from yellow to pale yellow. The maximum and minimum values of the refractive indices were measured in a (021) cleavage face using the immersion technique. The refractive indices of the liquids were checked using a Leitz-Jelley micro-refractometer with Na$_D$ at 26 °C. The measured extreme values are n_{min} = 1.657 and n_{max} = 1.660; this compares to an average refractive index calculated using the Gladstone-Dale relationship of $n^{mean}_{calc,Gladstone-Dale}$ = 1.65. The calculations are based on the assumption that Cr is present as chromate, with ρ = 2.84 g/cm^3, and using the average chemical analysis given in Table 1 corrected for the loss of water caused by the vacuum within the electron microprobe.

CHEMICAL COMPOSITION

The chemical composition of bouazzerite has been measured using a Cameca SX-51 electron microprobe (Table 1), under the following analytical conditions: accelerating voltage 15 kV, beam current 20 nA, counting times of 10 s on the peak and 5 s on each side of the peak for background, tightly focused beam scanned over a ~20 μm^2 surface, and with the following analytical standards: As, synthetic GaAs; Bi, synthetic Bi$_2$Se$_3$; Ca, wollastonite; Cr, crocoite; Mg, forsterite; Mn, rhodonite; Ni and Co, Ni-bearing cobaltite; Si, almandine garnet. The quality of the analyses is limited by the paucity of the available material, most of which was lost during polishing (very brittle material). The quality of the polish was also adversely affected by the shrinkage induced by the rapid dehydration caused by the vacuum inside the electron microprobe. The beam scanning averages any analytical effect that may result for the uneven surface. The resulting analytical totals, taking into account the water content

deducted from the crystal structure determination and analysis, are about 18 wt% too high; this indicates a vacuum-induced loss of about 56 H$_2$O per formula unit (pfu). Apart from the major constituents As, Bi, Fe, and Mg, bouazzerite contains minor (0.1 to 2 wt%) amounts of CoO, NiO, CaO, SiO$_2$, and Cr$_2$O$_3$ or CrO$_3$. Bond valence calculations (see below) indicate unambiguously that As and Fe are present as As^{5+} and Fe^{3+}, respectively.
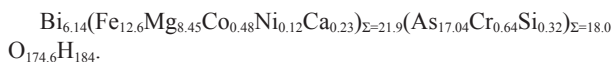
Chromium occurs in varying concentrations, corresponding to 0.35 to 1.03 atoms pfu; this element could not be located by the crystal structure refinement. Chromium may be present either at Cr^{3+} substituting for Fe^{3+} or Mg^{2+} in octahedral coordination (ionic radii: Cr^{3+} 0.62 Å; Mg^{2+} 0.72 Å; Fe^{3+} 0.55 Å; Shannon 1976), or as chromate ion Cr^{6+}O$_4^{2-}$ substituting for As^{5+}O$_4^{3-}$ (Cr^{6+} 0.26 Å; As^{5+} 0.34 Å). We discuss these two possibilities in the light of the geochemical conditions of growth for the new mineral and the correlation between the concentrations of the different metals in bouazzerite. Figure 2 shows the speciation of the three redox-sensitive constituents of bouazzerite: As, Cr, and Fe. Assuming that the oxidation state of As, Fe, and Cr in bouazzerite reflects essentially the oxidation state of these metals in the aqueous complexes from which it precipitated, Figure 2c indicates that the presence of significant quantities of Fe^{3+} in solutions requires highly oxidized conditions [presence of dissolved O$_2$(aq), for example] and an acidic pH (<4). Under these conditions, the model predicts that Cr may be present either as chromate or as Cr^{3+} (Fig. 2b).

The few available chemical analyses can be divided into two groups according to the Cr content; the Cr-rich composition is depleted in As and Fe, and the slope of the line joining both groups is about –1 when molar ratios are plotted (Figs. 3a and 3b). No such correlation is present for Mg (Fig. 3c). A possible coupled reaction to explain the observed correlation is

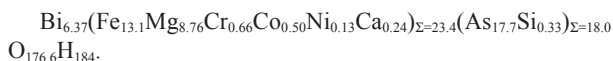$$CrO_4^{2-} + Mg^{2+} = AsO_4^{3-} + Fe^{3+} \tag{1}$$

The absence of correlation between Mg and Cr may result from the fact that most of the Mg is located on the Mg sites, and the Mg content is controlled by other, independent substitutions, that may involve vacancies and/or O^{2-}/OH$^-$/H$_2$O groups.

A full understanding of the role of Cr in the crystal structure of bouazzerite must await the availability of larger amounts of material. Assuming that Cr is incorporated following reaction 1, the empirical structural formula for bouazzerite is (normalization on 18 As + Cr + Si):

Bi$_{6.14}$(Fe$_{12.6}$Mg$_{8.45}$Co$_{0.48}$Ni$_{0.12}$Ca$_{0.23}$)$_{Σ=21.9}$(As$_{17.04}$Cr$_{0.64}$Si$_{0.32}$)$_{Σ=18.0}$O$_{174.6}$H$_{184}$.

If Cr is present as Cr^{3+} replacing Fe^{3+}, the empirical formula becomes

Bi$_{6.37}$(Fe$_{13.1}$Mg$_{8.76}$Cr$_{0.66}$Co$_{0.50}$Ni$_{0.13}$Ca$_{0.24}$)$_{Σ=23.4}$(As$_{17.7}$Si$_{0.33}$)$_{Σ=18.0}$O$_{176.6}$H$_{184}$.

In view of the analytical difficulties, these empirical formula compare favorably with the chemical formula retrieved from the single crystal solution (see below):

Bi$_6$(Mg,Co)$_{11}$Fe$_{14}$[AsO$_4$]$_{18}$O$_{174}$H$_{184}$.
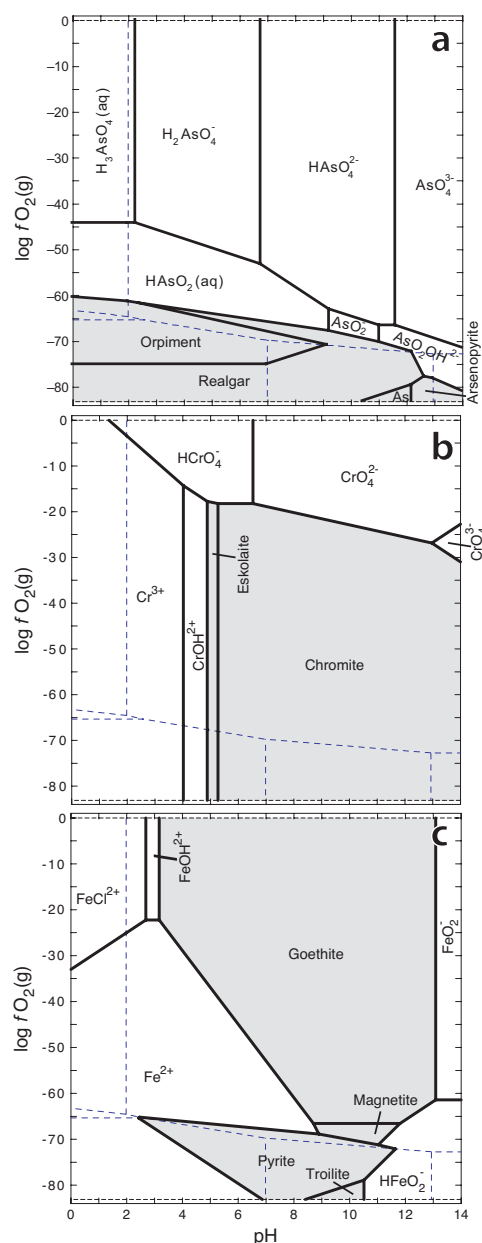
**FIGURE 2.** Log $f_{O_2}(g)$ vs. pH diagrams illustrating the speciation of As (**a**), Cr (**b**) and Fe (**c**) in groundwaters at 25 °C. The dashed lines on each diagram represent the sub-diagram for sulfur. Thermodynamic data were taken from the Lawrence Livermore database (LLNL V8 R6), as delivered with the Geochemist's Workbench software (Bethke 1996). The diagrams were drawn for the following conditions: $a\text{Cl}^- = 0.1$, activity of S species = 10^{-4}; (**a**) with activity of As species = 10^{-4}; (**b**) with activity of Cr = 10^{-8} and $a\text{Fe}^{2+} = 10^{-3}$; (**c**) with activity of Fe = 10^{-8}; hematite suppressed from the model.

CRYSTAL STRUCTURE

Data collection

A crystal of bouazzerite with approximate dimensions $0.12 \times 0.08 \times 0.04$ mm^3 was selected and mounted on a Bruker PLATFORM goniometer equipped with a 1K SMART CCD detector with a crystal-to-detector distance of 5 cm. The data
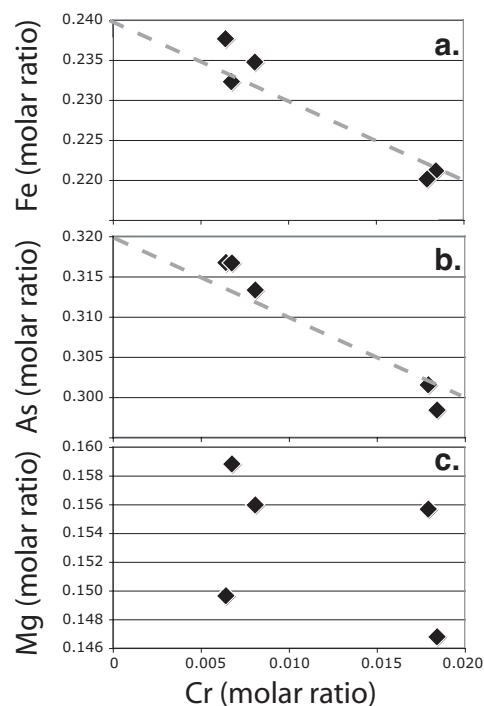
FIGURE 3. Bivariate diagrams illustrating the relationship between the Cr and Fe (**a**), As (**b**), and Mg (**c**) contents in bouazzerite, plotted in terms of molar ratios (wt% divided by molecular mass). The dashed lines in **a** and **b** have slopes of −1, indicating the trend expected for the coupled substitution $\text{CrO}_4^{2-} + \text{Mg}^{2+} = \text{AsO}_4^{3-} + \text{Fe}^{3+}$.

were collected using Mo$K\alpha$ X-radiation and frame widths of 0.3° in ω, with 45 s used to acquire each frame. More than a hemisphere of three-dimensional data was collected. The unit-cell dimensions were refined on the basis of 11 233 reflections using least-squares techniques (Table 2). The data were reduced and corrected for Lorentz, polarization, and background effects using the Bruker program SAINT. A semi-empirical absorption-correction based upon the intensities of equivalent reflections was done by modeling the crystal as an ellipsoid (program XPREP, part of the Bruker package). This reduced R_{int} of 778 intense reflections [$>10\sigma(I)$] from 22.4 to 5.7%.

Structure refinement

Scattering curves for neutral atoms, together with anomalous dispersion corrections, were taken from *International Tables for X-ray Crystallography*, vol. IV (Ibers and Hamilton 1974). The Bruker SHELXTL Version 5.1 set of programs was used for refinement of the crystal structure on the basis of F^2 (Sheldrick 1997). The structure was solved by direct methods. Refinement of all atom-position parameters, allowing for anisotropic displacement of all cations, and the inclusion of a weighting scheme of the structure factors, resulted in a final agreement index ($R1$) of 5.5%, calculated for the 7309 unique observed reflections ($|F_o| > 4\sigma_F$), and a goodness-of-fit (S) of 0.717. The final atomic parameters, isotropic displacement parameters, and the bond-valence values are listed in Table 3, the anisotropic displacement parameters for the cations are listed in Table 4 and selected interatomic distances are in Table 5. Observed and calculated structure factors are available from the authors upon request.

Cation coordination

AsO₄ polyhedra. The structure of bouazzerite contains nine different As sites. The bond valence sums for the As sites range from 4.80 to 5.11 v.u. (valence units), and the As-O bond distances range from 1.637 to 1.730 Å. The average As-O bond distances in the AsO_4^{3-} tetrahedra vary over a very short range: 1.68 to 1.70 Å. The O15 (1.31 v.u., bound to the As6 atom), O19 (1.44 v.u., bound to As7), O21 (1.26 v.u., bound to As9), and O47 (1.28 v.u., bound to As8) sites have low bond valence sums. However, they are considered as O atoms as they form the shortest As-O bonds in their respective AsO₄ tetrahedra and therefore it is highly unlikely that these sites are protonated. Low bond-valence sums are typical for terminal O atoms of arsenate and phosphate groups if they are involved in strong hydrogen bonding to adjacent H_2O or OH groups (Krivovichev et al. 2002). In the case of bouazzerite, four above mentioned O atoms form either two or three short O···H_2O contacts of 2.59–2.78 Å that are indicative of moderately strong hydrogen bonds. The bond valences of the respective H bonds can be estimated as 0.20–0.30 v.u., which complements the observed bond-valence sums of the terminal O atoms to a total of 2 v.u.

Bi(O,H₂O)₆₋₈ polyhedra. There are three independent Bi sites: Bi1 is surrounded by 7 O atoms (2.139 to 3.058 Å), Bi2 is surrounded by 6 O atoms (2.156 to 2.962 Å), and Bi3 is surrounded by 7 O atoms (2.131 to 3.285 Å) and one H_2O group at 2.830 Å. The coordination of the Bi^{3+} cations is strongly distorted owing to the stereochemical activity of the $6s^2$ lone electron pairs. All three Bi atoms form five strong Bi^{3+}-O bonds of 2.13–2.64 Å located in one coordination hemisphere and complemented by several additional weak bonds longer than 2.83 Å. The bond valence sums for Bi are 3.05 to 3.17 v.u.

Mg(O,H₂O)₆ polyhedra. There are 6 independent Mg sites. The occupancy of the Mg1 site refines to 1.36 using the atom scattering curve of Mg; this indicates that Co substitutes mainly on this site, with an occupancy corresponding to $Mg_{0.76}Co_{0.24}$. Because the total amount of Co is 0.48 atoms pfu according to chemical analysis in Table 1, some Co may occur in a disordered

fashion in the other Mg sites as well. All Mg sites are octahedrally coordinated, and Mg is bound to oxygen atoms and either 4 (Mg1, Mg3, Mg4) or 5 (Mg2, Mg5, Mg6) H_2O molecules. The Mg-O bond distances are between 2.015 and 2.10 Å, and the Mg-H_2O bond distances between 2.03 and 2.17 Å. The bond valence sums for the Mg sites are between 1.98 and 2.10 v.u., and the bond valence sums for the H_2O molecules bound to Mg are 0.28 to 0.46 v.u.

FeO₆ polyhedra. There are seven independent Fe sites. Six of these sites are octahedrally coordinated to 6 O atoms at distances between 1.922 to 2.117 Å, with average Fe-O bond distances between 2.01 and 2.02 Å. The Fe5 site is in near-perfect trigonal
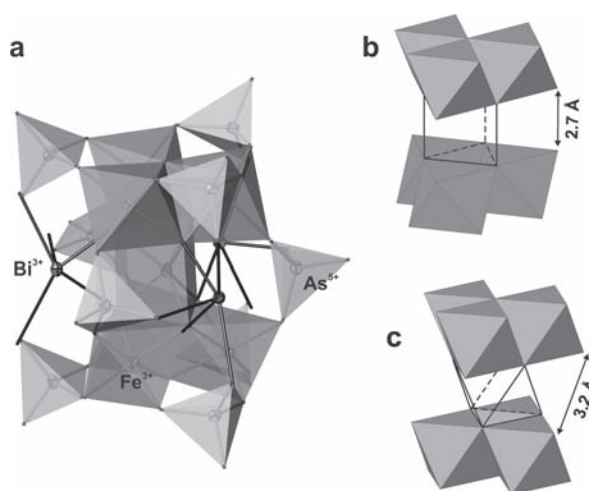

FIGURE 4. The $[Bi_3Fe_7O_6(OH)_2(AsO_4)_9]^{11-}$ nanocluster in the structure of bouazzerite (**a**) and two schemes used to explain trigonal prismatic coordination of the Fe5 site (**b**, **c**). See text for details.

TABLE 2. Crystallographic data and refinement parameters for bouazzerite

a (Å)	13.6322(13)
b (Å)	30.469(3)
c (Å)	18.4671(18)
β (°)	91.134(2)
V (Å³)	7669.0(13)
Space group	$P2_1/n$
Z	2
F_{000}	6066
μ (cm⁻¹)	121.99
D_{calc} (g/cm³)	2.81
Crystal size (mm³)	0.12 × 0.08 × 0.04
Radiation	Mo$K\alpha$
2θ max	56.72°
Total ref.	45206
Unique ref.	17318
Unique $|F_o| \geq 4\sigma_F$	7309
No. refined parameters	574
R_1	0.055
wR_2	0.076
GooF	0.717
Weighting scheme	$a = 0$; $b = 0$

Note: $R_1 = \Sigma||F_o| - |F_c||/\Sigma|F_o|$; $wR_2 = \{\Sigma[w(F_o^2 - F_c^2)^2]/\Sigma[w(F_o^2)^2]\}^{1/2}$; $w = 1/[\sigma^2(F_o^2) + (a*P)^2 + b*P]$, $P = [Max (F_o^2, 0) + 2*F_c^2]/3$; $S = \{\Sigma[w(F_o^2 - F_c^2)]/(n-p)\}^{1/2}$, where $n = 7309$ is the number of reflections and $p = 574$ is the number of refined parameters.
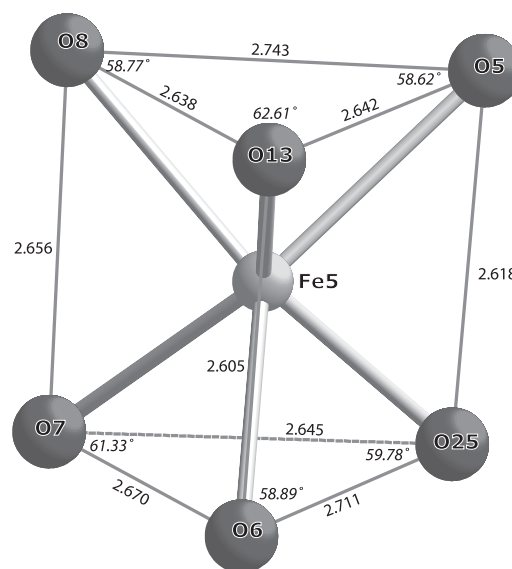

FIGURE 5. Coordination around the Fe5 site in the structure of bouazzerite.

TABLE 3. Fractional atomic coordinates and displacement parameters

Atom	x	y	z	U_{eq} (Å²)	BVS (v.u.)*	Atom	x	y	z	U_{eq} (Å²)	BVS (v.u.)*
Bi1	0.33234(4)	0.439265(17)	0.05963(3)	0.01694(14)	3.05	O32	0.2901(6)	0.3281(3)	0.3822(4)	0.023(2)	1.88
Bi2	0.38659(4)	0.271567(17)	0.19862(3)	0.01812(14)	3.11	O33	0.4650(7)	0.3243(3)	0.0504(5)	0.028(2)	1.94
Bi3	0.35259(4)	0.423520(17)	0.37927(3)	0.01714(14)	3.17	O34	0.0698(6)	0.4430(3)	0.3039(4)	0.019(2)	1.68
As1	0.61733(10)	0.45153(4)	0.36421(7)	0.0172(3)	4.96	O35	0.4876(6)	0.3343(3)	0.3752(4)	0.024(2)	1.83
As2	0.32019(11)	0.50594(4)	0.25068(7)	0.0177(3)	5.07	O36	0.2727(7)	0.3094(3)	0.0754(5)	0.025(2)	1.94
As3	0.39425(11)	0.29800(4)	0.38449(7)	0.0173(3)	5.02	O37	0.2315(6)	0.2254(3)	0.2110(4)	0.023(2)	1.49
As4	0.35232(11)	0.32830(4)	0.01404(7)	0.0183(4)	5.11	O38	0.3258(7)	0.5597(3)	0.2553(4)	0.026(2)	1.79
As5	0.09272(10)	0.42095(4)	0.38783(7)	0.0168(3)	4.80	O39	0.6383(6)	0.3963(3)	0.3561(4)	0.018(2)	1.72
As6	0.12300(11)	0.25221(4)	0.21955(8)	0.0184(4)	4.87	O40	0.3912(6)	0.2613(3)	0.3141(4)	0.020(2)	2.01
As7	0.58885(11)	0.44700(4)	0.04135(7)	0.0172(3)	4.87	H₂O41	0.2649(7)	0.6473(3)	0.2237(5)	0.027(2)	0.34
As8	0.64960(11)	0.27860(5)	0.20621(8)	0.0205(4)	4.90	H₂O42	0.4774(7)	0.6339(3)	0.2394(5)	0.031(3)	0.40
As9	0.06318(10)	0.42076(4)	0.05797(7)	0.0173(3)	4.80	H₂O43	0.1706(6)	0.5226(3)	−0.0833(4)	0.023(2)	0.35
Fe1	0.19098(15)	0.33957(6)	0.30552(10)	0.0196(5)	3.06	H₂O44	0.2973(7)	0.4515(3)	−0.1091(5)	0.032(3)	0.32
Fe2	0.55546(15)	0.35884(6)	0.29353(10)	0.0183(5)	3.06	H₂O45	0.3853(7)	0.2589(3)	−0.1963(5)	0.026(2)	0.39
Fe3	0.15471(14)	0.42957(6)	0.21954(10)	0.0187(5)	3.01	H₂O46	0.4260(7)	0.5459(3)	0.4350(5)	0.039(3)	0.34
Fe4	0.54076(15)	0.35731(6)	0.12029(10)	0.0187(5)	3.07	O47	0.7550(7)	0.2506(3)	0.2001(5)	0.030(3)	1.28*
Fe5	0.35571(14)	0.37933(6)	0.21313(10)	0.0153(5)	2.87	O48	0.4075(6)	0.4869(3)	0.1955(4)	0.022(2)	1.88
Fe6	0.51905(15)	0.44607(6)	0.20669(10)	0.0198(5)	3.05	H₂O49	0.2109(7)	0.2349(3)	0.5216(5)	0.034(3)	0.31
Fe7	0.17860(15)	0.34025(6)	0.13515(10)	0.0198(5)	3.06	H₂O50	−0.1601(7)	0.4707(3)	0.5362(5)	0.027(2)	0.36
Mg1†	1/2	1/2	1/2	0.022(2)	2.10	H₂O51	−0.1913(7)	0.3913(3)	0.4357(5)	0.033(3)	0.30
Mg2	0.1429(3)	0.45627(13)	−0.1023(2)	0.0119(10)	2.02	O52	0.3438(6)	0.3007(3)	−0.0626(5)	0.022(2)	1.80
Mg3	0.3684(3)	0.60454(14)	0.1802(2)	0.0215(12)	2.06	H₂O53	0.3954(7)	0.2249(3)	0.6036(5)	0.036(3)	0.35
Mg4	−0.1410(3)	0.45746(14)	0.4274(2)	0.0180(11)	1.98	O54	0.5528(7)	0.2445(3)	0.2139(5)	0.029(3)	1.65
Mg5	0.3529(4)	0.21064(14)	0.4977(2)	0.0224(12)	2.01	H₂O55	−0.0882(7)	0.5232(3)	0.4247(5)	0.029(3)	0.31
Mg6	0.3875(3)	0.23984(14)	−0.0901(2)	0.0212(12)	2.09	H₂O56	0.2431(7)	0.2182(3)	−0.0983(5)	0.036(3)	0.35
O1	0.4783(6)	0.4497(3)	−0.0015(4)	0.019(2)	1.76	H₂O57	−0.0102(7)	0.4652(3)	−0.1074(5)	0.032(3)	0.32
OH2	0.1044(6)	0.3655(2)	0.2227(4)	0.014(2)	1.29	H₂O58	0.4272(7)	0.1750(3)	−0.1263(5)	0.030(3)	0.28
O3	0.6527(7)	0.3118(3)	0.2806(5)	0.022(2)	1.75	H₂O59	0.6318(7)	0.5347(3)	0.4841(5)	0.028(2)	0.46
O4	0.1250(7)	0.2827(3)	0.2975(5)	0.024(2)	1.74	H₂O60	0.5391(7)	0.2558(3)	−0.0870(5)	0.028(3)	0.32
O5	0.4385(6)	0.4054(2)	0.1342(4)	0.011(2)	2.03	O61	0.1509(6)	0.4456(3)	0.0088(4)	0.021(2)	1.57
O6	0.2755(6)	0.3241(2)	0.2206(4)	0.014(2)	2.05	H₂O62	−0.1199(7)	0.4568(3)	0.3128(5)	0.032(3)	0.30
O7	0.2560(6)	0.4007(2)	0.2890(4)	0.013(2)	2.00	H₂O63	0.3986(7)	0.2165(3)	0.0168(5)	0.034(3)	0.33
O8	0.4512(6)	0.4076(2)	0.2826(4)	0.014(2)	2.06	H₂O64	0.3988(7)	0.6489(3)	0.0916(5)	0.038(3)	0.28
O9	0.1032(6)	0.3652(3)	0.3775(4)	0.020(2)	1.71	H₂O65	0.4886(7)	0.1848(3)	0.4749(5)	0.041(3)	0.37
H₂O10	0.4777(6)	0.5628(3)	0.1400(4)	0.025(2)	0.33	H₂O66	0.3128(7)	0.1456(3)	0.5293(5)	0.037(3)	0.30
O11	0.0602(6)	0.4449(3)	0.1418(4)	0.020(2)	1.73	H₂O67	0.2574(7)	0.5805(3)	0.1094(5)	0.039(3)	0.32
O12	0.0876(6)	0.3659(3)	0.0648(4)	0.022(2)	1.78	H₂O68	0.1341(8)	0.4598(3)	−0.2162(5)	0.048(3)	0.32
O13	0.4661(6)	0.3331(3)	0.2109(4)	0.016(2)	2.04	H₂O69	0.3000(8)	0.1981(3)	0.3935(5)	0.047(3)	0.35
O14	0.4045(6)	0.2715(3)	0.4614(4)	0.020(2)	1.75	H₂O70	0.1369(8)	0.3884(3)	−0.1066(6)	0.053(3)	0.36
O15	0.0294(7)	0.2170(3)	0.2220(5)	0.026(2)	1.31*	H₂O71	−0.0910(7)	0.3445(3)	0.2200(5)	0.038(3)	–
O16	0.2111(6)	0.4876(3)	0.2163(4)	0.021(2)	1.83	H₂O72	0.7911(7)	0.4167(3)	0.1951(5)	0.036(3)	–
O17	0.5982(6)	0.4741(3)	0.2807(4)	0.019(2)	1.83	H₂O73	0.6594(7)	0.6333(3)	0.1730(5)	0.038(3)	–
OH18	0.6067(6)	0.3917(2)	0.2046(4)	0.014(2)	1.34	H₂O74	−0.2016(8)	0.4103(3)	0.6398(5)	0.051(3)	–
O19	0.6770(6)	0.4706(3)	−0.0058(4)	0.017(2)	1.44*	H₂O75	0.2544(8)	0.1745(3)	0.0891(5)	0.046(3)	–
O20	0.5169(6)	0.4587(3)	0.4137(4)	0.020(2)	1.66	H₂O76	0.0392(8)	0.5398(3)	0.3011(6)	0.059(3)	–
O21	−0.0482(6)	0.4262(3)	0.0181(4)	0.018(2)	1.26*	H₂O77	0.5131(8)	0.1416(3)	0.0439(6)	0.055(3)	–
O22	−0.0018(6)	0.4317(3)	0.4429(4)	0.022(2)	1.60	H₂O78	0.1989(8)	0.3255(3)	0.5219(5)	0.050(3)	–
O23	0.3384(6)	0.4883(3)	0.3369(4)	0.021(2)	2.12	H₂O79	0.6083(9)	0.2018(4)	0.3542(6)	0.064(4)	–
O24	0.5867(6)	0.4720(3)	0.1235(4)	0.015(2)	1.76	H₂O80	0.4075(9)	0.6305(4)	0.4859(6)	0.065(4)	–
O25	0.2465(6)	0.3997(3)	0.1458(4)	0.018(2)	2.01	H₂O81	0.1155(8)	0.2354(3)	0.0102(6)	0.059(3)	–
O26	0.3199(6)	0.3811(3)	−0.0049(4)	0.021(2)	2.08	H₂O82	0.5475(11)	0.6775(4)	0.4092(7)	0.103(5)	–
O27	0.7147(6)	0.4750(3)	0.4033(4)	0.019(2)	1.79	H₂O83	0.7577(12)	0.6598(5)	0.2972(8)	0.126(6)	–
O28	0.1967(6)	0.4413(3)	0.4252(4)	0.018(2)	1.73	H₂O84	0.0722(11)	0.6223(5)	0.1897(8)	0.108(5)	–
O29	0.1023(6)	0.2859(3)	0.1477(4)	0.025(2)	1.77	H₂O85	0.5205(14)	0.1556(6)	0.1892(9)	0.156(7)	–
O30	0.6178(6)	0.3920(3)	0.0510(4)	0.021(2)	1.66	H₂O86	0.6604(16)	0.6117(6)	0.4151(11)	0.193(9)	–
O31	0.6379(6)	0.3103(3)	0.1311(4)	0.021(2)	1.80	H₂O87	0.3013(16)	0.4441(7)	−0.2934(10)	0.194(9)	–

* Bond-valences calculated using parameters taken from Brown and Altermatt (1985); contributions from hydrogen bonds are not included; despite low bond-valence sums, the O15, O19, O21, and O47 sites are considered as O atoms as they form shortest As-O bonds in the respective AsO₄ tetrahedra.
† Occupancy: Mg₀.₇₆Co₀.₂₄.

prismatic coordination (Figs. 4 and 5), with 6 O atoms located between 2.004 and 2.075 Å, and an average Fe-O bond distance of 2.03. Bond valence sums indicate clearly that iron is trivalent on all the 7 sites (2.87 v.u. on Fe5 to 3.06 v.u.).

STRUCTURE DESCRIPTION

The crystal structure of bouazzerite is based upon $[Bi_3Fe_7O_6(OH)_2(AsO_4)_9]^{11-}$ anionic nanoclusters shown in Figure 4a. The cluster is centered around a $[^{trigonal\ prismatic}Fe^{3+}(^{octahedral}Fe_3^{3+}(OH)O_{12})_2]$ group, containing one Fe^{3+} ion in near-ideal trigonal prismatic coordination (Fig. 5) and 6 Fe^{3+} ions in octahedral coordination.

The nanoclusters have a diameter of about 1.3 nm and are linked together by chains of $Mg(H_2O)_6$ octahedra. Each of the three $Bi(O,H_2O)_{6-8}$ polyhedrons shares an edge with the trigonal prism around the Fe5 site, and two apexes with two arsenate tetrahedra linked to octahedral Fe sites. The resulting arrangement displays channels down [100] that contain structural water (Fig. 6).

X-ray powder diffraction study

The X-ray powder-diffraction pattern of bouazzerite (Table 6) was measured with a 114.6 mm diameter Gandolfi camera using Mn-filtered Cu$K\alpha$ radiation (40 kV, 30 mA; 50 h

TABLE 4. Anisotropic displacement parameters (Å^2) of cations in the structure of bouazzerite

Atom	U_{11}	U_{22}	U_{33}	U_{23}	U_{13}	U_{12}
Bi1	0.0176(3)	0.0157(3)	0.0176(3)	0.0013(2)	0.0009(2)	0.0002(2)
Bi2	0.0204(3)	0.0149(3)	0.0191(3)	−0.0009(2)	0.0010(3)	0.0006(2)
Bi3	0.0179(3)	0.0178(3)	0.0158(3)	−0.0004(2)	0.0010(2)	0.0000(2)
As1	0.0141(9)	0.0202(9)	0.0173(9)	−0.0036(6)	0.0001(7)	0.0001(6)
As2	0.0188(9)	0.0158(9)	0.0187(9)	−0.0002(6)	0.0015(7)	−0.0005(6)
As3	0.0194(9)	0.0168(8)	0.0158(9)	0.0023(6)	0.0000(7)	0.0027(6)
As4	0.0213(9)	0.0175(9)	0.0161(9)	−0.0012(6)	−0.0003(7)	0.0027(6)
As5	0.0144(9)	0.0189(9)	0.0171(8)	−0.0020(6)	0.0016(6)	0.0017(6)
As6	0.0209(9)	0.0145(8)	0.0199(9)	0.0018(6)	0.0021(7)	−0.0016(6)
As7	0.0165(9)	0.0188(9)	0.0165(9)	−0.0001(6)	0.0013(7)	−0.0013(6)
As8	0.0194(9)	0.0221(9)	0.0199(9)	0.0010(7)	0.0007(7)	0.0060(7)
As9	0.0164(9)	0.0178(8)	0.0176(8)	0.0009(6)	−0.0001(7)	0.0014(7)
Fe1	0.0202(13)	0.0187(12)	0.0200(12)	0.0006(9)	0.002(1)	−0.0001(9)
Fe2	0.0183(13)	0.0199(12)	0.0166(12)	−0.0007(9)	0.0008(9)	0.0010(9)
Fe3	0.0192(13)	0.0182(12)	0.0188(12)	−0.0006(9)	0.0024(9)	0.0006(9)
Fe4	0.0191(13)	0.0189(12)	0.0182(12)	0.0013(9)	0.0017(10)	0.0020(9)
Fe5	0.0179(13)	0.0139(12)	0.0141(12)	0.0014(8)	0.0002(9)	0.0017(9)
Fe6	0.0177(13)	0.0219(13)	0.0197(12)	−0.0006(9)	0.0014(9)	0.0011(9)
Fe7	0.0193(13)	0.0183(12)	0.0218(13)	−0.0002(9)	0.002(1)	0.0000(9)
Mg1	0.020(4)	0.027(4)	0.018(3)	−0.002(2)	−0.001(2)	−0.002(2)
Mg2	0.016(3)	0.011(3)	0.009(3)	0.0012(19)	0.002(2)	0.0024(19)
Mg3	0.024(3)	0.017(3)	0.025(3)	−0.001(2)	0.009(2)	−0.003(2)
Mg4	0.019(3)	0.015(3)	0.020(3)	−0.007(2)	0.000(2)	0.003(2)
Mg5	0.027(3)	0.020(3)	0.020(3)	0.005(2)	0.001(2)	0.000(2)
Mg6	0.020(3)	0.023(3)	0.021(3)	−0.002(2)	0.000(2)	0.001(2)

TABLE 5. Selected bond lengths (Å) in the structure of bouazzerite

Bond	Length	Bond	Length	Bond	Length
Bi1-O26	2.139(8)	As7-O19	1.661(8)	Fe6-O17	1.924(9)
Bi1-O5	2.230(8)	As7-O1	1.691(9)	Fe6-O24	1.972(8)
Bi1-O1	2.328(8)	As7-O24	1.699(8)	Fe6-O48	1.972(9)
Bi1-O25	2.330(8)	As7-O30	1.730(8)	Fe6-O18	2.044(8)
Bi1-O61	2.635(9)	<As7-O>	1.70	Fe6-O8	2.060(8)
Bi1-O19	2.922(8)			Fe6-O5	2.117(8)
Bi1-O48	3.058(9)	As8-O47	1.677(9)	<Fe6-O>	2.01
<Bi1-O>	2.52	As8-O54	1.688(9)		
		As8-O31	1.696(8)	Fe7-O12	1.942(9)
Bi2-O40	2.156(8)	As8-O3	1.707(8)	Fe7-O36	1.950(8)
Bi2-O13	2.176(8)	<As8-O>	1.69	Fe7-O29	1.973(8)
Bi2-O6	2.246(8)			Fe7-O25	2.043(8)
Bi2-O54	2.423(9)	As9-O21	1.682(9)	Fe7-O2	2.072(8)
Bi2-O37	2.553(8)	As9-O61	1.694(8)	Fe7-O6	2.097(8)
Bi2-O36	2.962(9)	As9-O12	1.708(8)	<Fe7-O>	2.01
<Bi2-O>	2.42	As9-O11	1.716(8)		
		<As9-O>	1.70	Mg1-O20	2.047(8)
Bi3-O23	2.131(8)			Mg1-O20	2.047(8)
Bi3-O7	2.216(8)	Fe1-O4	1.958(8)	Mg1-H₂O46	2.09(1)
Bi3-O8	2.308(7)	Fe1-O9	1.967(8)	Mg1-H₂O46	2.09(1)
Bi3-O28	2.366(8)	Fe1-O32	1.970(9)	Mg1-H₂O59	2.111(9)
Bi3-O20	2.553(9)	Fe1-O6	2.020(8)	Mg1-H₂O59	2.111(9)
Bi3-H₂O59	2.830(9)	Fe1-O2	2.070(8)	<Mg1-O>	2.08
Bi3-O32	3.030(8)	Fe1-O7	2.087(8)		
Bi3-O35	3.285(8)	<Fe1-O>	2.01	Mg2-H₂O70	2.07(1)
<Bi3-O>	2.59			Mg2-O61	2.080(9)
		Fe2-O35	1.935(8)	Mg2-H₂O43	2.085(9)
As1-O27	1.659(9)	Fe2-O39	1.965(9)	Mg2-H₂O57	2.11(1)
As1-O20	1.675(8)	Fe2-O3	1.969(9)	Mg2-H₂O68	2.11(1)
As1-O17	1.704(8)	Fe2-O18	2.057(8)	Mg2-H₂O44	2.12(1)
As1-O39	1.715(8)	Fe2-O8	2.063(8)	<Mg2-O>	2.10
<As1-O>	1.69	Fe2-O13	2.086(9)		
		<Fe2-O>	2.01	Mg3-H₂O42	2.03(1)
As2-O38	1.642(8)			Mg3-O38	2.040(9)
As2-O48	1.685(8)	Fe3-O16	1.930(8)	Mg3-H₂O41	2.09(1)
As2-O23	1.694(8)	Fe3-O11	1.966(9)	Mg3-O10	2.105(9)
As2-O16	1.699(9)	Fe3-O34	2.002(8)	Mg3-H₂O67	2.11(1)
<As2-O>	1.68	Fe3-O7	2.063(8)	Mg3-H₂O64	2.17(1)
		Fe3-O2	2.071(8)	<Mg3-O>	2.09
As3-O14	1.637(8)	Fe3-O25	2.077(8)		
As3-O32	1.690(9)	<Fe3-O>	2.02	Mg4-O22	2.07(1)
As3-O35	1.697(9)			Mg4-H₂O50	2.070(9)
As3-O40	1.713(8)	Fe4-O33	1.922(9)	Mg4-O27	2.08(1)
<As3-O>	1.68	Fe4-O31	1.957(9)	Mg4-H₂O55	2.13(1)
		Fe4-O30	1.977(8)	Mg4-H₂O51	2.14(1)
As4-O52	1.648(8)	Fe4-O5	2.041(8)	Mg4-H₂O62	2.14(1)
As4-O33	1.669(10)	Fe4-O18	2.068(8)	<Mg4-O>	2.11
As4-O36	1.686(8)	Fe4-O13	2.108(8)		
As4-O26	1.704(8)	<Fe4-O>	2.01	Mg5-H₂O65	2.06(1)
<As4-O>	1.68			Mg5-H₂O53	2.08(1)
		Fe5-O8	2.004(8)	Mg5-H₂O69	2.08(1)
As5-O28	1.683(9)	Fe5-O6	2.013(8)	Mg5-O14	2.099(9)
As5-O22	1.688(8)	Fe5-O25	2.019(9)	Mg5-H₂O49	2.13(1)
As5-O34	1.712(8)	Fe5-O5	2.023(7)	Mg5-H₂O66	2.14(1)
As5-O9	1.717(8)	Fe5-O13	2.062(8)	<Mg5-O>	2.10
<As5-O>	1.70	Fe5-O7	2.075(8)		
		<Fe5-O>	2.03	Mg6-O52	2.015(9)
As6-O15	1.668(9)			Mg6-H₂O45	2.04(1)
As6-O29	1.697(9)			Mg6-H₂O56	2.08(1)
As6-O37	1.700(9)			Mg6-H₂O63	2.10(1)
As6-O4	1.712(8)			Mg6-H₂O60	2.12(1)
<As6-O>	1.69			Mg6-H₂O58	2.16(1)
				<Mg6-O>	2.09

exposure time). The intensities were visually estimated. The calculated intensities were obtained from the structural model. The eight strongest lines in the X-ray powder diffraction pattern are [d in Å(I)(hkl)]: 11.79(100)(02$\bar{1}$), 10.98(80)(101/$\bar{1}$01), 10.16(80)($\bar{1}$20), 7.900(80)(02$\bar{2}$), 12.45(70)(1$\bar{1}$0), 15.78(60)(0$\bar{1}$1), 3.414(40)(3$\bar{3}$3/400), 3.153(40)(35$\bar{3}$/2$\bar{2}$5). Least-squares refinement of the powder diffraction data using the program UnitCell (Holland and Redfern 1997) and 19 unambiguously indexed lines gave the following unit-cell parameters: $a = 13.58(2)$ Å, $b = 30.62(4)$ Å, $c = 18.49(2)$ Å, $\beta = 90.9(1)°$. The theoretical d-spacings and intensities listed in Table 6 were calculated for the formula $Bi_6Mg_{11}Fe_{14}(AsO_4)_{18}O_{12}(OH)_4(H_2O)_{86}$ with the program Crystal Diffract of D.C. Palmer (www.crystalmaker.com).

DISCUSSION

Relations to other species

Chemically, bouazzerite is related to several Bi arsenates (Table 7), including two polymorphs of $BiAsO_4$ (rooseveltite and tetrarooseveltite) and several compounds including cations such as Al^{3+}, Pb^{2+}, Cu^{2+}, Ni^{2+}, Fe^{3+}, and uranyl. Bouazzerite is the only Bi-arsenate mineral that contains both Mg and Fe^{3+} as essential constituents.

Structurally, bouazzerite is a new compound with a unique crystal structure that has no close topological relation with any known mineral or synthetic compound structure. Among Bi-arsenates, the nano-porous nature of bouazzerite is shared by mixite, $BiCu_6(OH)_6(AsO_4)_3 \cdot nH_2O$ (Mereiter and Preisinger 1986; Miletich et al. 1997), but the diameter of the channels is much smaller in bouazzerite (~4.8 Å in diameter) than in mixite (9.5 Å). Apart from mixite, hydrated Bi-arsenate minerals display a layer structure (Table 7). Bouazzerite is the first Bi-arsenate to be built around nano-clusters.

Coordination of Fe^{3+} and the trigonal prismatic geometry

A unique feature of the structure of bouazzerite is the presence of Fe^{3+} in trigonal prismatic coordination. The trigonal prismatic coordination is rare, and for a long time was known only in the crystal lattices of some heavy metal sulfides (e.g., MoS_2 and WS_2). Arsenic in nickeline, NiAs, also occurs in near-trigonal prismatic coordination. In general, the trigonal prismatic coordination results in lower ligand field stabilization energy than the octahedral coordination, never higher (Gillum et al. 1970).
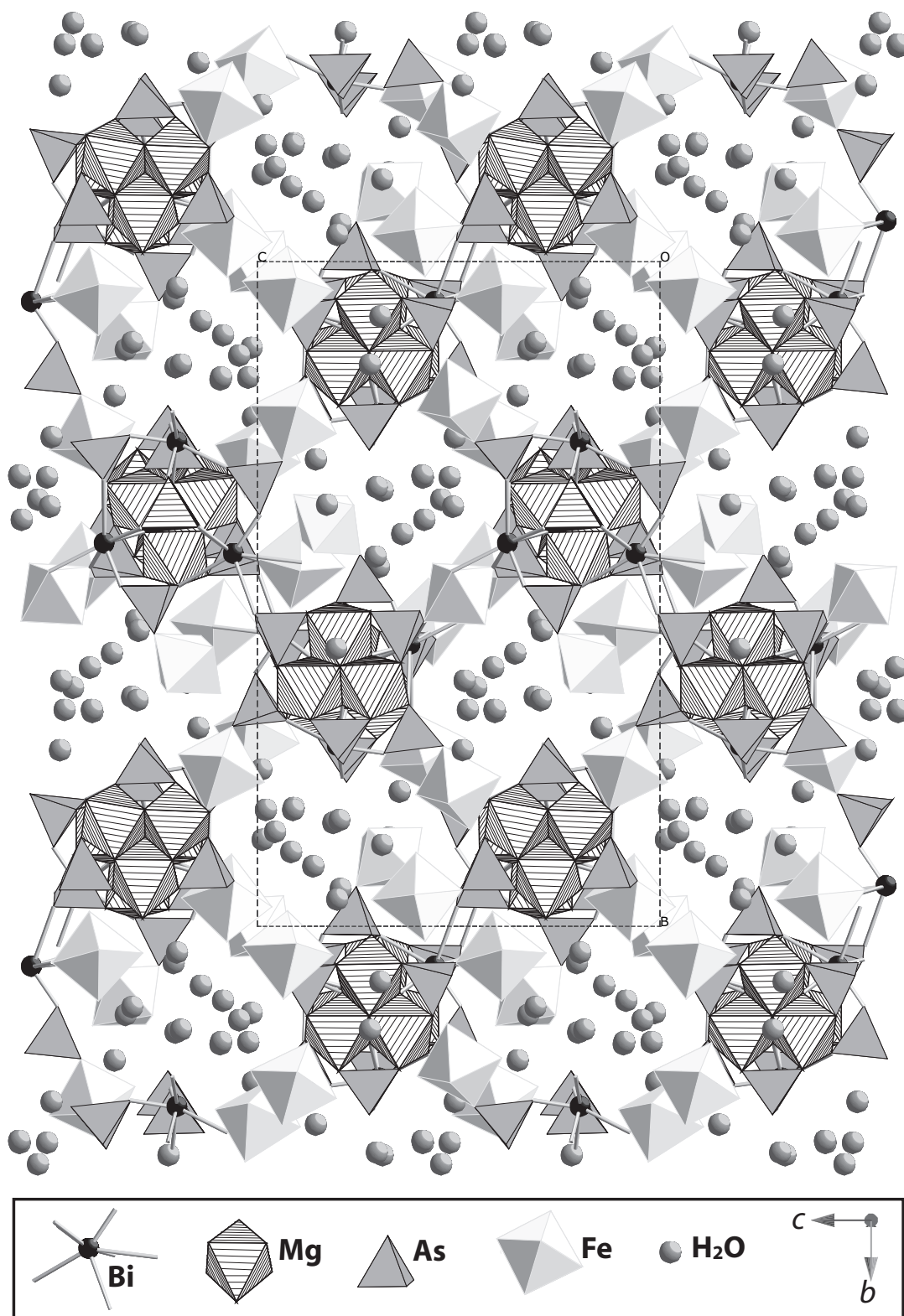
FIGURE 6. Projection of the crystal structure of bouazzerite on (100). Hatched octahedra are $Mg(O,H_2O)_6$, filled tetrahedra are AsO_4, filled octahedra are $Fe^{3+}O_6$, spheres with bonds are $Bi(O,H_2O)_{6-8}$ polyhedra. Only the isolated H_2O groups bonded only by hydrogen bonding are shown individually.

TABLE 6. X-ray powder data for bouazzerite

hkl	d_{obs} (Å)	I_{obs}	d_{calc} (Å)	I_{calc}
$0\bar{1}1$	15.78	60	15.79	12
$1\bar{1}0$	12.45	70	12.44	32
$02\bar{1}$	11.79	100	11.75	100
$\bar{1}01$			11.07	15
101	10.98	80 broad	10.86	31
$\bar{1}20$	10.16	80	10.16	29
$02\bar{2}$	7.900	80	7.895	7
$02\bar{3}$	5.717	20	5.706	4
060	5.096	10	5.078	4
$\bar{1}33$	4.942	10	4.938	3
$04\bar{3}$	4.796	10	4.787	5
$21\bar{3}$	4.552	10	4.561	1
$\bar{2}50$			4.543	1
$14\bar{3}$	4.484	10	4.495	2
310			4.494	2
$3\bar{2}1$	4.220	30	4.220	1
$03\bar{4}$			4.202	5
$04\bar{4}$	3.952	20 broad	3.948	1
$2\bar{4}3$	3.875	20	3.889	0.3
105	3.555	10 broad	3.547	1
$3\bar{3}3$	3.414	40	3.411	3
400			3.407	5
$\bar{3}61$	3.339	10	3.339	2
$4\bar{3}0$	3.215	20	3.230	4
$35\bar{3}$	3.153	40	3.157	3
$2\bar{2}5$			3.150	1
$1\bar{8}3$			3.144	5
370			3.143	2
016			3.062	4
$3\bar{4}4$	2.954	30 broad	2.955	1
$\bar{4}23$			2.949	1
036			2.945	1
$\bar{4}51$			2.944	1
$3\bar{2}5$	2.836	20 broad	2.843	1
$4\bar{3}3$			2.839	0.4
305			2.838	0.4
$3\bar{5}4$			2.838	0.4
$4\bar{6}0$			2.829	2
$05\bar{6}$	2.755	10	2.747	5
$43\bar{4}$	2.629	<10	2.624	2
$3\bar{9}2$	2.600	<10	2.596	1
			2.522	10
$3\bar{9}3$	2.475	10	2.473	1
$1\,\overline{12}\,1$			2.472	1
416	2.254	10	2.255	1
$4\bar{9}3$	2.233	10	2.227	2

Notes: X-ray diffraction powder pattern of bouazzerite measured with a Gandolfi camera, 114.6 mm in diameter; Mn-filtered Cu$K\alpha$/X-ray radiation; generator operated at 40 kV, 30 mA; 50 h exposure time. Intensities were visually estimated. The calculated intensities are for the crystal structure model.

TABLE 7. Bismuth arsenate minerals

Asselbornite	$(Pb,Ba)(UO_2)_6(BiO)_4(AsO_4)_2(OH)_{12}\cdot3H_2O$	Sarp et al. 1983
Atelestite	$Bi_8[O_5(OH)_5(AsO_4)_3]$	Mereiter and Preisinger 1986
Cobaltneustädtelite	$Bi_2Fe^{3+}(Co,Fe^{3+})_2[(O,OH)|OH|AsO_4]_2$	Krause et al. 2002
Medenbachite	$Bi_2Fe^{3+}(Cu,Fe^{2+})(O,OH)_2(AsO_4)_2$	Krause et al. 1996
Mixite	$BiCu_6^{2+}(AsO_4)_3(OH)_6\cdot3H_2O$	Miletich et al. 1997
Neustädtelite	$Bi_2Fe^{3+}(Fe^{3+},Co)_2[(O,OH)|OH|AsO_4]_2$	Krause et al. 2002
Orthowalpurgite	$(BiO)_4(UO_2)(AsO_4)_2\cdot2H_2O$	Krause et al. 1995
Paganoite	$NiBi[O|AsO_4]$	Roberts et al. 2001
Petitjeanite	$(Bi,Pb)_3O(PO_4,AsO_4)_2(OH)$	Krause et al. 1993
Preisingerite	$Bi_3O(OH)(AsO_4)_2$	Bedlivy and Mereiter 1982a
Rooseveltite	α-$BiAsO_4$	Bedlivy and Mereiter 1982b
Schumacherite	$Bi_3O(VO_4,AsO_4,PO_4)_2(OH)$	Walenta et al. 1983
Tetrarooseveltite	β-$Bi(AsO_4)$	Sejkora and Ridkosil 1994
Walpurgite	$(UO_2)Bi_4O_4(AsO_4)_2\cdot2H_2O$	Mereiter 1982

a trigonal prismatic void at the center. The second configuration (Fig. 4c) has an inversion center located in between the trimers and has an octahedral void. In the first case, O atoms of the basal planes of the FeO_6 octahedra are separated by ~2.7 Å, whereas, in the second the O-O distance is approximately 3.2 Å (calculated using ideal octahedral geometry and average Fe-O distances). The configuration shown in Figure 4b is therefore appropriate for the attachment of an arsenate tetrahedron with the O···O distances of ~2.6–2.8 Å, whereas the configuration in Figure 4c is not. Thus it is very likely that the trigonal prismatic coordination is a consequence of steric constraints that are imposed by the presence of the same AsO_4^{3-} groups as ligands for Fe^{3+} ions of adjacent octahedral trimers. Therefore, the observed stabilization of the trigonal prismatic coordination is due to the ridigity of arsenate groups.

It is of interest that the $[Bi_3Fe_7O_6(OH)_2(AsO_4)_9]^{11-}$ nanoclusters have almost perfect hexagonal symmetry $\bar{6}$ with very small deviations from an ideal geometry. These deviations are induced by the presence of the Mg^{2+} ions and H_2O molecules that prevent the nanoclusters to crystallize in an ideal symmetry environment.

The significance of the Bi-As-Fe nanoclusters in bouazzerite

Bouazzerite is the first mineral based upon complex Bi- and As-containing ferric nanoclusters. Although heterometal oxoions play an important role in coordination chemistry, their importance in natural environments is poorly understood (e.g., recent review by Casey 2005). The discovery of the Bi-As-Fe^{3+} clusters in bouazzerite suggests that similar clusters may be present in the oxidation zone of ore deposits and in acid mine drainage waters, contributing to the mobility and toxicity of metals in these environments. Al^{3+} clusters of similar size have been reported to occur in solutions from forested soils (Hunter and Ross 1991). The fact that the cluster present in bouazzerite has no equivalent in synthetic compounds opens the way to the synthesis of new compounds, possibly with interesting properties (e.g., Nyman et al. 2002).

At least one example of first row transition metal coordinated by 6 oxygen atoms in trigonal prismatic arrangement is known: $[Co^{2+}(Co^{3+}(OCH_2CH_2NH_2)_3)_2]^{2+}$, in which it is believed that the trigonal prism is favored over a third octahedron because of interligand repulsion in the latter (Bertrand et al. 1969; Huheey 1983). An alternative way to stabilize the trigonal prismatic coordination is to tailor the ligand to be rigid and to favor this geometry (Wentworth 1972). For example, this is achieved for Fe^{2+} in the complex $[Fe^{2+}CXO_3(BC_6H_5)(HCOC_2H_5)_3]^+$, where CXO is cyclohexanedion-1, 2-monooxime hydrazone (Voloshin et al. 1999). In this complex, Fe^{2+} is coordinated by six N atoms in near-trigonal prismatic geometry.

It is very likely that the trigonal prismatic coordination of the Fe5 site in bouazzerite is also the result of ligand interactions. Figures 4b and 4c show two configurations that result from different packing modes of trimers of FeO_6 octahedra. The first configuration (Fig. 4b) has a horizontal mirror plane and creates

to Philippe Thélin (XRD laboratory, Institute of Mineralogy and Geochemistry, UNIL, Lausanne) for providing XRD-powder micro-analysis facilities. Robert (Bob) Pecorini was the collecting fellow who accompanied one of the authors (G.F.) to Bou Azzer when the new mineral was found. The manuscript benefited from the comments from two reviewers, Luca Bindi and Herta Effenberger, and from the associate editor, Giacomo Diego Gatta.

REFERENCES CITED

Bedlivy, D. and Mereiter, K. (1982a) Preisingerite, $Bi_3O(OH)(AsO_4)_2$, a new species from San Juan Province, Argentina: its description and crystal structure. American Mineralogist, 67, 833–840.

——— (1982b) Structure of BOX-$BiAsO_4$ (rooseveltite). Acta Crystallographica, B38, 1559–1561.

Bertrand, J.A., Kelley, J.A., and Vassian, E.G. (1969) Trigonal prismatic cobalt(II) in a polynuclear complex. Journal of the American Chemical Society, 91, 2394–2395.

Bethke, C.M. (1996) Geochemical reaction modeling, concepts and applications, 397 p. Oxford University Press, New York.

Birch, W.D., Pring, A., Reller, A., and Schmalle, H. (1993) Bernalite, $Fe(OH)_3$, a new mineral from Broken Hill, New South Wales: description and structure. American Mineralogist, 78, 827–834.

Brown, I.D. and Altermatt, D. (1985) Bond-valence parameters obtained from a systematic analysis of the inorganic crystal structure database. Acta Crystallographica, B41, 244–248.

Caillères, S. (1942) Stichtite collected in the serpentinite massif of Bou Azzer at Bou Oufroh. Bulletin de la Société Française de Minéralogie et Cristallographie, 65, 135–136.

Casey, W.H. (2005) Large aqueous aluminum hydroxide molecules. Chemical Reviews, 1–16.

Cesbron, F.P., Ginderow, D., Giraud, R., Pelisson, P., and Pillard, F. (1987) Nickelaustinite $Ca(Ni,Zn)(AsO_4)(OH)$, a new mineral species from the cobalto-nickeliferous district of Bou-Azzer, Morocco. Canadian Mineralogist, 25, 401–407.

Dunn, P.J., Sturman, B.D., and Nelen, J.A. (1987) Wendwilsonite, the Mg analogue of roselite, from Morocco, New Jersey, and Mexico, and new data on roselite. American Mineralogist, 72, 217–221.

Favreau, G. and Dietrich, J.E. (2001) Le district cobalto-nickélifère de Bou Azzer (Maroc). Géologie, histoire et description des espèces minérales. Bulletin de l'Association Française de Microminéralogie, 73, 111 p.

——— (2006) Die Mineralien von Bou Azzer. Lapis, 31, 27–68.

Fleischer, M. (1957) Smolianinovite (abstract). American Mineralogist, 42, 307–308.

Gillum, W.O., Wentworth, R.A.D., and Childers, R.F. (1970) Hindered ligand systems. IV. Complexes of *cis*,*cis*-1,3,5-*tris*(pyridine-2-carboxaldimino) cyclohexane. Trigonal-prismatic vs. octahedral coordination. Inorganic Chemistry, 9, 1825–1832.

Holland, T.J.B. and Redfern, S.A.T. (1997) Unit cell refinement from powder diffraction data: the use of regression diagnostics. Mineralogical Magazine, 61, 65–77.

Huheey, J.E. (1983) Inorganic chemistry. Principles of structure and reactivity, 936 p. Harper and Row Publishers, New York.

Hunter, D. and Ross, D.S. (1991) Evidence for a phytotoxic hydroxy-aluminium polymer in organic soil horizons. Science, 251, 1056–1058.

Ibers, J.A. and Hamilton, W.C. (1974) International tables for X-ray crystallography, Vol. IV. The Kynoch Press, Birmingham, U.K.

Jacob, C. and Schubnel, H.-J. (1972) Erythrite from Bou-Azzer, Anti-Atlas. Notes et Mémoires du Service Géologique (Rabat), 32, 154 p. Rabat, Morocco.

Krause, W., Belendorff, K., and Bernhardt, H.J. (1993) Petitjeanite, $Bi_3O(OH)(PO_4)_2$, a new mineral, and additional data for the corresponding arsenate and vanadate, preisingerite and schumacherite. Neues Jahrbuch für Mineralogie-Monatshefte, 487–503.

Krause, W., Effenberger, H., and Brandstätter, F. (1995) Orthowalpurgite, $(BiO)_4(UO_2)(AsO_4)_2\cdot2H_2O$, a new mineral from the Black Forest, Germany. European Journal of Mineralogy, 7, 1313–1324.

Krause, W., Bernhardt, H.J., Gebert, W., Graetsch, H., Belendorff, K., and Petitjean, K. (1996) Medenbachite, $Bi_2Fe(Cu,Fe)(O,OH)_2(OH)_2(AsO_4)_2$, a new mineral species: Its description and crystal structure. American Mineralogist, 81, 505–512.

Krause, W., Bernhardt, H.J., McCammon, C., and Effenberger, H. (2002) Neustädtelite and cobaltneustädtelite, the Fe^{3+}- and Co^{2+}-analogues of medenbachite. American Mineralogist, 87, 726–738.

Krause, W., Bernhard, H.-J., Effenberger, H., Kolitsch, U., and Lengauer, C. (2003) Redefinition of arhbarite, $Cu_2Mg(AsO_4)(OH)_3$. Mineralogical Magazine, 67, 1099–1107.

Krivovichev, S.V., Britvin, S.N., Burns, P.C., and Yakovenchuk, V.N. (2002) Crystal structure of rimkorolgite, $Ba[Mg_5(H_2O)_7(PO_4)_4](H_2O)$, and its comparison with bakhchisaraitsevite. European Journal of Mineralogy, 14, 397–402.

Leblanc, M. (1980) Cobalt and nickel. In Gîtes minéraux. Notes et Mémoires du Service Féologique du Maroc., 157–182.

Leblanc, M. and Billaud, P. (1982) Cobalt arsenide orebodies related to an Upper Proterozoic ophiolite—Bou-Azzer (Morocco). Economic Geology, 77, 162–175.

Meisser, N. and Brugger, J. (2006) Bouazzerite and maghrebite, two new minerals from the Bou Azzer district, Morocco. Lapis, 31, 69–71.

Mereiter, K. (1982) The crystal-structure of walpurgite, $(UO_2)Bi_4O_4(AsO_4)_2\cdot2H_2O$. Tschermaks Mineralogische und Petrographische Mitteilungen, 30, 129–139.

Mereiter, K. and Preisinger, A. (1986) Kristallstrukturdaten der Wissmutminerale Atelestit, Mixit und Pucherit. Österrische Akademie Wissenschaft, Mathematisch-Naturwissenschaft Klasse, 123, 79–81.

Miletich, R., Zemann, J., and Nowak, M. (1997) Reversible hydration in synthetic mixite, $BiCu_6(OH)_6(AsO_4)_3\cdot nH_2O$ ($n \leq 3$): hydration kinetics and crystal chemistry. Physics and Chemistry of Minerals, 24, 411–422.

Nyman, M., Bonhomme, F., Alam, T.M., Rodriguez, M.A., Cherry, B.R., Krumhansl, J.L., Nenoff, T.M., and Sattler, A.M. (2002) A general synthetic procedure for heteropolyniobates. Science, 297, 996–998.

Paclt, J. (1953) Second report about mineral nomenclature. Neues Jahrbuch für Mineralogie. Monatshefte, 188–190.

Pierrot, R. and Schubnel, H.-J. (1972) L'irhtemite, un nouvel arséniate hydraté de calcium et magnésium. Bulletin de la Societé Française de Minéralogie, 92, 365–370.

Pring, A. (1995) The place of descriptive mineralogy in modern science. The Australian Mineralogist, 1, 3–7.

Roberts, A.C., Burns, P.C., Gault, R.A., Criddle, A.J., and Feinglos, M.N. (2001) Paganoite, $NiBi^{3+}As^{5+}O_5$, a new mineral from Johanngeorgenstadt, Saxony, Germany: description and crystal structure. European Journal of Mineralogy, 13, 167–175.

Sarp, H., Bertrand, J., and Deferne, J. (1983) Asselbornite, $(Pb,Ba)(UO_2)_6(BiO)_4[(As,P)O_4]_2(OH)_{12}\cdot3H_2O$, a new uranium, bismuth, lead and barium hydrous arsenate. Neues Jahrbuch für Mineralogie, Monatshefte, 417–423.

Schmetzer, K., Tremmel, G., and Medenbach, O. (1982) Arhbarite, $Cu_2[OH|AsO_4]\cdot6H_2O$, a new mineral from Bou Azzer, Morocco. Neues Jahrbuch für Mineralogie, Monatshefte, 529–533.

Sejkora, J. and Ridkosil, T. (1994) Tetrarooseveltite, β-$Bi(AsO_4)$, a new mineral species from Moldava deposit, the Krusne-Hory Mountains, Northwestern Bohemia, Czech-Republic. Neues Jahrbuch für Mineralogie, Monatshefte, 179–184.

Shannon, R.D. (1976) Revised effective ionic radii and systematic studies of interatomic distances in halides and chalcogenides. Acta Crystallographica, A32, 751–767.

Sheldrick, G.M. (1997) SHELXL-97, Program for the refinement of crystal structures. Universität Göttingen, Germany.

Voloshin, Y.Z., Stash, A.I., Varzatskii, O.A., Belsky, V.K., Maletin, Y.A., and Strizhakova, N.G. (1999) New capping agents for oximehydrazonate clathrochelates: sterically controlled synthesis, structural characterization and intramolecular reactions. Inorganica Chimica Acta, 284, 180–190.

Walenta, K., Dunn, P.J., Hentschel, G., and Mereiter, K. (1983) Schumacherite, a new bismuth mineral from Schneeberg in Saxony. Tschermaks Mineralogische und Petrographische Mitteilungen, 31, 165–173.

Welch, M.D., Crichton, W.A., and Ross, N.L. (2005) Compression of the perovskite-related mineral bernalite $Fe(OH)_3$ to 9 GPa and a reappraisal of its structure. Mineralogical Magazine, 69, 309–315.

Wentworth, R.A.D. (1972) Trigonal prismatic vs. octahedral stereochemistry in complexes derived from innocent ligands. Coordination Chemistry Reviews, 1–2, 171–187.

Williams, P.A. (1990) Oxide zone geochemistry, 286 p. Ellis Horwood, New York.